On the influence of graphene oxide and hydroxyapatite modification on alginate-based hydrogel matrix: thermal, physicochemical, and biological considerations

Aleksandra Lach[1] · Monika Skoczeń[1] · Klaudia Ordon[1] · Patrycja Domalik-Pyzik[1] · Sylwia Noga[2,3] · Małgorzata Sekuła-Stryjewska[3] · Elżbieta Karnas[2] · Aleksandra Byrska[2] · Joanna Jagiełło[4] · Ludwika Lipińska[4] · Ewa Zuba-Surma[2] · Kinga Pielichowska[1]

Abstract

Sodium alginate (SA) hydrogels with an addition of graphene oxide (GO) and hydroxyapatite (HAp) crosslinked by calcium chloride solution were investigated as potential materials for osteochondral tissue regeneration. The influence of various ratios of the nanoadditives in the natural derived polymer matrix on the thermal, physiochemical and biological properties was studied. Two thermal characterization methods (DSC and TGA) were employed to examine the thermal properties of the materials and provide information regarding the different types of water within the hydrogel structure. These parameters are crucial for the assessing and understanding of the adsorption/desorption processes in hydrogels and also impact their biocompatibility. The effect of GO and HAp addition on thermal characteristics of alginate hydrogel is reported, as well as the nanoadditives polymer chains interaction, as evidenced by FTIR results. The compression test confirmed that the nanoadditives, uniformly dispersed in the polymer matrix, improved the mechanical properties of the hydrogels, but only up to a certain content of additives. The composite hydrogels exhibited a very low friction coefficient. Both GO and HAp also enhanced chemical stability of alginate hydrogels under in vitro conditions. Biological assays demonstrated that most of the tested hydrogel extracts were not cytotoxic to hUC-MSCs, but they can affect the proliferation rate of the cells. Developed materials may present an intriguing alternative for osteochondral tissue regeneration.

Keywords Thermal characterization · Hydrogels · Sodium alginate · Graphene oxide · Hydroxyapatite

Introduction

The osteochondral tissue consists of cartilage, calcified cartilage and subchondral bone layers with different chemical, microstructural, mechanical and biological properties. The cartilage layer contains mainly collagen type II, glycosaminoglycans and water. In deeper layers, cartilage gradually changes to a calcified cartilage composed of type II collagen, glycosaminoglycans, hydroxyapatite and water. Calcified cartilage is an interface between cartilage and bone that allows the structural continuity [1, 2]. Beneath the calcified cartilage is the porous subchondral bone, mainly composed of type I collagen, glycosaminoglycans, hydroxyapatite (up to 40%), and much smaller amount of water, up to a few percent [3]. Cartilage is a connective tissue composed of small cells called chondrocytes, which are surrounded by ECM (Extracellular Matrix). Cartilage is mostly aneural and avascular. Its most abundant form is hyaline (articular)

✉ Ewa Zuba-Surma
  ewa.zuba-surma@uj.edu.pl

✉ Kinga Pielichowska
  kingapie@agh.edu.pl

1 Department of Biomaterials and Composites, Faculty of Materials Science and Ceramics, AGH University of Krakow, Al. Mickiewicza 30, 30-059 Krakow, Poland

2 Department of Cell Biology, Faculty of Biochemistry, Biophysics and Biotechnology, Jagiellonian University, Gronostajowa 7, 30-387 Krakow, Poland

3 Malopolska Centre of Biotechnology, Jagiellonian University, Gronostajowa 7a, 30-387 Krakow, Poland

4 Department of Chemical Synthesis and Flake Graphene, Łukasiewicz Research Network-Institute of Microelectronics and Photonics, Al. Lotników 32/46, 02-668 Warsaw, Poland

cartilage, which is located at the ends of long bones and takes part in musculoskeletal movement. Cartilage, especially in knee joints, is exposed to comprehensive stresses, such as compressive force and shear stress at cartilage bone boundary. That is why damages of this tissue are very common, particularly among physically active, obese or elderly people [4, 5]. The biggest problem is that cartilage tissue has very low self-healing ability. In addition, because cartilage is aneural, it is very hard to detect its defects. Only when the damage comes deeper to the subchondral bone (full thickness defects), a patient feels pain and new solutions to face this problem are needed [4]. The commonly used materials for cartilage tissue regeneration are polymers, due to their low density, degradability which can be easily controlled and more environmental friendly effects [6]. Articular cartilage can be described as a composite which consists up to 80% of water in the structure. That is why most commonly used materials are polymeric hydrogels, especially the natural ones [5].

Lately, alginate hydrogels have gained an increased attention in the biomedical field, due to their biocompatibility, non-toxicity, biodegradability and ability to facilitate the regeneration process of a tissue. Alginate is a linear polysaccharide, which is built from β-D-mannuronic acid (M blocks) and α-L-guluronic acid (G blocks) residues. In the presence of divalent cations alginates undergo sol–gel transition. For biomedical applications mostly Ca^{2+} cations are used for crosslinking [7, 8]. The biggest disadvantage of alginates (and natural polymers in general) is their low mechanical strength making modification desirable [6].

Alginate hydrogels in cartilage regeneration were investigated by Al-Sabah et al. [9] who manufactured nanocellulose-based hydrogels combined with crosslinked sodium alginate. Stagnaro et al. [10] obtained alginate-polymethacrylate hybrid hydrogel; whereas, Radhakrishnan et al. [11] prepared alginate/PVA hydrogels with chondroitin sulfate nanoparticles (ChS-NPs) in chondral and nanohydroxyapatite (nHA) in subchondral zone. Injectable growth factor-loaded affinity-binding alginate hydrogels were obtained by Ruvinov et al. [12], and Montalbano et al. [13] prepared a tri-component hydrogel using collagen, alginate and fibrin. Zhu et al. [14] proposed a bilayer material: SA/bioglass hydrogel into which bone marrow stem cells (BMSCs) were added (for subchondral bone regeneration) and thermosensitive SA/agarose (AG) with co-culture of BMSCs and articular chondrocytes (ACs) for articular cartilage regeneration.

Graphene oxide (GO) contains functional groups like hydroxyl, epoxide, carbonyl and carboxylic on the basal planes and edges. The presence of these groups improves interaction between GO and alginate matrix due to the electrostatic interactions [15]. Marrella et al. [16] investigated hydrogel made from 2% alginate solution modified with GO. An addition of GO provided better mechanical properties and viability of cells. Increase of tensile properties was also proved by Serrano-Aroca et al. [17]. According to Ionita et al. [18], addition of GO not only improves mechanical properties of alginate films, but also their thermal stability. Shamekhi et al. [19] showed that incorporation of GO in concentration from 0 to 0.1, 0.2 and 0.3% considerably enhanced physical and mechanical properties. Additionally, an increased proliferation with augmentation of the GO percentage of the human articular chondrocytes on the nanocomposite was observed.

HAp is widely used for bone regeneration, because of similar mineral composition. In addition, usage of HAp in biomaterial can promote osteogenesis and osteointegration [20]. Jiang et al. [21] obtained alginate-based hydrogels modified with HAp nanowires, which showed improved mechanical properties (with respect to pure SA) and high biocompatibility. Rajkumar et al. [22] manufactured an alginate/HAp composite and their results confirmed good interaction between polymer and ceramic particles, which caused good mechanical properties of the composite.

Based on the literature, it was found that there is no work that describes this topic in a thorough manner. In this work, both GO- and HAp-modified alginate hydrogels were described. Most of the already published research works is focused on the composite films characterization, while in this paper bulk materials were manufactured and investigated by using various methods, including methods not commonly utilized in this field of research, such as tribological measurements. The commonly applied methods, such as FTIR and DSC, have been extended in this paper with a detailed analysis of the distance and energy of hydrogen bonds and the information on different types of water in polymer hydrogels. Hence, we believe that this work provides a comprehensive approach for characterization of modified alginate hydrogel materials.

In this paper, we report on a biomimetic strategy to prepare layers for multi-layered scaffolds for possible use in osteochondral tissue engineering. The alginate hydrogels were modified either with graphene oxide (GO) or hydroxyapatite (HAp). These additives were used to obtain hydrogel scaffolds suitable for regeneration of hyaline cartilage or calcified cartilage and bone tissue, respectively. Alginate hydrogels were crosslinked with calcium chloride ($CaCl_2$) aqueous solution. The influence of various ratios of nanoadditives in the polymer matrix on its properties was examined in order to obtain materials suitable for osteochondral tissue regeneration.

Materials and methods

Materials

Sodium alginate (Lot Number A0386291) in the form of light yellow–brown powder with a viscosity of 500 mPa·s

(1% at 20 °C, Brookfield LV) and pH of 7.03 (1% at 20 °C) was purchased from Acros ORGANICS (Geel, Belgium). Based on the relationship of density (ρ) and flow time (t) between the solution and the solvent, the inherent viscosity η_{inh} was evaluated using the Eq. (1):

$$\eta_{inh} = \frac{\eta - \eta_0}{\eta_0} = \frac{t\rho - t_0\rho_0}{t_0\rho_0} \tag{1}$$

where η and η_0 are the viscosities of the solution and the pure solvent, respectively; t and t_0 are the flow times of the solution and the solvent, respectively; ρ and ρ_0 are the densities of the solution and the solvent, respectively. Assuming that $\rho \cong \rho_0$ and $\rho_0 = 1.00 g\,cm^{-3}$ the Eq. (2) is given by:

$$\eta_{inh} \cong \frac{t - t_0}{t_0} \tag{2}$$

Next, the intrinsic viscosity [η] was evaluated. According to Huggins [23] [η] is defined by the Eq. (3):

$$[\eta] \cong \lim_{c \to 0} \frac{\eta_{inh}}{c} \tag{3}$$

The intercept of a plot of η_{inh} versus concentration (c) is related to the intrinsic viscosity, [η]. Based on the intrinsic viscosity an average M_η was calculated using the Eq. (4):

$$M_\eta = \left\{ \frac{[\bar\eta]}{K} \right\}^{\frac{1}{a}} \tag{4}$$

Where $K = 0.0123 cm^3\,g^{-1}$ and $a = 0.96$ [24]. For sodium alginate used in the course of this work, the calculated M_η was 7895 g mol^{-1}. By using the method proposed by Sakugawa et al. [25] the determined mannuronate/glucoronate ratio for sodium alginate was 1:1.

Dehydrated calcium chloride in the form of powder was purchased from POCH Avantor Performance Materials Poland S.A. (Gliwice, Poland). As nanoadditives graphene oxide and hydroxyapatite were used. GO in the form of paste was supplied from Łukasiewicz Research Network-Institute of Microelectronics and Photonics (Łukasiewicz IMiF, Warsaw, Poland). The GO was produced by modified Hummers method using graphite flakes as starting material [26]. 1 g of paste contained 19.2 mg of GO in the form of flakes. Hydroxyapatite needle like shape (60 nm) was purchased from mkNano (Mississauga, Canada).

Preparation of the hydrogels

Before the preparation of composite hydrogels, the trial series without additives was made. Manufactured hydrogels were mechanically tested in order to choose the concentration of polymer and crosslinking agent for which hydrogel has the best mechanical parameters, such as Young modulus and compression strength. Based on these results, the second series of hydrogels with constant concentration of sodium alginate (3%mass) and calcium chloride (0.075 M) and various concentrations of GO and HAp were manufactured (Table 1.).

The composite hydrogels were obtained as follows: into the polypropylene containers 25 mL of 3.6% SA aqueous solution was poured. Nanoadditives were dispersed by sonication in 5 mL of distilled water and added to the SA solution. The samples were degassed in the vacuum dryer. Next, 90 mL of 0.075 M calcium chloride aqueous solution was added. The samples were gently mixed using glass rod in order to obtain spherical-like shape hydrogel samples with a diameter of ca. 3 cm. The samples were left in the CaCl$_2$ solution for at least one week to obtain fully crosslinked hydrogels.

Viscosity-average molecular mass of sodium alginate

To determinate the viscosity-average molecular mass (M_η) of sodium alginate (SA), five aqueous solutions were prepared with concentration of 0.1, 0.15, 0.2, 0.25 and 0.3%. The flow time was determined at room temperature (25 °C) using Ubbelohde viscometer with a water flow of 31 s. The measurement was performed three times for each solution, then the average flow time was calculated.

Thermal analysis (DSC and TG)

DSC measurements were performed using DSC1 from Mettler Toledo (Columbus, OH, USA). For the measurement, ca. 3.5 mg of the samples were put into the pierced aluminum pans. Samples were heated from −30 °C to 200 °C with 10 °C min^{-1} heating rate under a nitrogen atmosphere (30 mL min^{-1}).

In order to determine water content in the hydrogels and the temperature of their thermal degradation, TG tests using TGA550 Discovery thermogravimetric analyzer from TA Instruments (New Castle, DE, USA) was performed. For the measurement, ca. 15–20 mg of the samples were put

Table 1 Composition of the obtained hydrogels

Concentration		Modifying phase used in hydrogels	
Sodium alginate %	Calcium chloride M	GO/%	HAp/%
3	0.075	0.1	1
		0.2	2
		0.5	5
		1	10
		1.5	15
		3	30

into the platinum open pans. Samples were heated from 30 to 500 °C with 10 °C min^{-1} heating rate under a nitrogen atmosphere (25 mL min^{-1}). Peak deconvolution was done using OriginPro software.

Spectroscopic analysis (FTIR)

FTIR measurements were performed using Tensor 27 spectrometer from Bruker (Billerica, MA, USA) in KBr pellets at 2 cm^{-1} resolution in the range of 4000–400 cm^{-1}. Before measurement, spherical samples were cut, lyophilized and dried in the vacuum dryer.

Mechanical properties

Mechanical test was performed using Zwick 1435 machine from Zwick Roell (Ulm, Germany) according to the PN-EN ISO 604 standard. Before the measurements, $10 \times 10 \times 10$ mm cubic specimens were cut. The specimens were compressed with a 1–3.5 kN force and 2 mm s^{-1} deformation speed. Each measurement was ended when deformation of the sample reached 6 mm. Based on the results from three measurements per sample, average Young modulus and compressive strength were determined. Also, exact dimensions of the specimens were measured before and after compression. Based on this, average Poisson ratio was calculated using the equation:

$$v = -\frac{\left(\frac{\Delta d}{d}\right)}{\left(\frac{\Delta L}{L}\right)} \tag{5}$$

Where d and Δd represent the dimension of the sample in the compression axis and the change after the measurement, respectively; L and ΔL represent the dimension of the sample perpendicular to the compression axis and the change after the measurement, respectively. The final Poisson ratio is an average from the result obtained along the compression axis and the axis perpendicular to it.

Tribological properties

Tribology measurements were carried out using MCR302 modular compact rheometer (Anton Paar, Graz, Austria) equipped with T-PTD 200 tribology cell. The ball-on-three plates was a geometry of choice as a well-established method for measuring different tribological systems. Unhardened stainless steel ball (diameter of ½", SP-BC12.7/1.4401 GRADE 100, 41,514, Anton Paar) and three polytetrafluoroethylene (PTFE) plates (dimensions of $6 \times 15 \times 3$ mm, SP-BC6-15-3/PTFE, 79,726, Anton Paar) were used for each measurement as tribopairs. Approximately 4–5 mL of

non-crosslinked material was loaded into the tribology cell; the ball was then lowered onto the plates to reach a normal force of 5N, subsequently the pot was covered with a lid. The sliding velocity increased from 0.1 to 1000 mm s^{-1}, the Stribeck curve was recorded at 5 N load, the temperature was set and maintained (dedicated Peltier system) at 36 °C to imitate human body temperature. A minimum of five repetitions were carried out for each material.

Microscopic analysis (SEM)

Microscopic observations were made using NOVA nanoSEM 200 Scanning Electron Microscope from FEI Europe B.V. (Eindhoven, The Netherlands) with 18 kV electron beam energy. For the measurement, lyophilized samples were covered by carbon and examined with the magnification 350×.

Chemical stability under in vitro conditions

In vitro chemical stability was tested according to EN ISO 10993-13 using Ringer and PBS solution at 37 °C. The samples before the incubation weighed ca. 5–6 g. Every 3–4 days solution pH and sample mass was measured. Ringer solution was obtained in the shape of pills from MERCK (Darmstadt, Germany) and dissolved in 1 l of distilled water according to the recipe given by the producer (the final molarity was: 154 mM NaCl, 5.6 mM KCl, 2.2 mM $CaCl_2$ anhydrous, and 2.4 mM $NaHCO_3$). PBS was made from: 8 g NaCl; 0.2 g KCl; 1.44 g Na_2HPO_4 and 0.24 g KH_2PO_4 and fulfilled with distilled water up to 1L (the resulting molarity was: 137 mM NaCl, 2.7 mM KCl, 10 mM Na_2HPO_4, and 1.8 mM KH_2PO_4).

Isolation, culture and phenotype characterization of hUC-MSCs

Human umbilical cord-derived MSCs (hUC-MSCs) were isolated from umbilical cord Wharton's Jelly by explant method. Umbilical cords were provided by The Polish Stem Cell Bank (Warsaw, Poland), which is a partner in this project. Isolated cells were cultured in tissue culture flasks (Eppendorf, Hamburg, Germany) in DMEM/F12 (Sigma-Aldrich, St. Louis, MI, USA) medium supplemented with 10% fetal bovine serum (FBS; Sigma-Aldrich, St. Louis, MI, USA), 100 µg mL^{-1} penicillin and 10 µg mL^{-1} streptomycin solution (P/S; Thermo Fisher Scientific, Waltham, MA, USA) at 37 °C in a humidified atmosphere with 5% CO_2. For the phenotype characterization, the hUC-MSCs were harvested with TrypLE (Thermo Fisher Scientific, Waltham, MA, USA) solution at passage 3–4. Cells were stained with fluorescent-labeled antibodies directed to CD14, CD16, CD34 (all FITC-labeled; BD Biosciences, Franklin Lakes,

NJ, USA), CD73, CD90, CD105, HLA-DR (all PE-labeled; Biolegend, San Diego, CA, USA) and CD29 (PE-Cy-5; Biolegend, San Diego, CA, USA). All antibodies were used according to manufacturer's immunostaining protocols. Surface markers on hUC-MSC were detected using the BD LSRFortessa flow cytometer (Becton Dickinson, Franklin Lakes, NJ, USA) with FACSDiva software (Becton Dickinson, Franklin Lakes, NJ, USA). Cells from 4 to 7 passages were used in experiments.

Cytotoxicity assay

Based on the standards and guidelines included in the ISO 10993 Norm, dedicated for the biological evaluation of potential medical devices, materials extracts were prepared for indirect cytotoxicity assay. 50 mg mL^{-1} mass to volume ratio of the hydrogel in DMEM/F12 was used for each extract. After 24 h of incubation, the extracts were collected and prepared for the biological assays.

The potential cytotoxicity of alginate extracts on hUC-MSCs was examined by measuring the level of lactate dehydrogenase (LDH) released from damaged cells. We used the Cytotoxicity Detection Kit (Roche Diagnostics, Rotkreuz, Switzerland), according to the manufacturer's protocol. hUC-MSCs were passaged with TrypLE (Thermo Fisher Scientific, Waltham, MA, USA) solution and seeded at 4×10^3 density into a 96-well plate (Eppendorf, Hamburg, Germany) in 150 µL of standard culture medium. After 6 h of incubation at 37 °C the culture medium was changed to 150 µl of each alginate extracts supplemented with 2% FBS and $1 \times$ P/S. After 24 h of hUC-MSCs incubation, the plate was centrifuged at $300 \times$ g for 5 min. Next, 100 µl of the supernatant from each well was transferred to new 96-well plate (Eppendorf, Hamburg, Germany). Subsequently, the 100 µl of LDH-substrate mixture was added to the each supernatant. After 30 min. of incubation in dark at room temperature, the absorbance at 450 nm and 620 nm with a microplate reader Multiskan FC (Thermo Fisher Scientific, Waltham, MA, USA) was measured. The cells cultured on TC-treated polystyrene surface (TCPS) in standard medium were used as a control.

Cell proliferation assay

To evaluate the influence of alginate extracts on hUC-MSCs proliferation capacity, the colorimetric assay Cell Counting Kit-8 (CCK-8, Sigma-Aldrich, St. Louis, MI, USA) was performed. hUC-MSCs were passaged with TrypLE solution (Thermo Fisher Scientific, Waltham, MA, USA) and seeded at 4×10^3 density into a 96-well plate (Eppendorf, Hamburg, Germany) in 100 µl of standard culture medium. After 6 h of incubation at 37 °C the culture medium was changed to 100 µl of alginate extract supplemented with 10% FBS and

$1 \times$ P/S. The proliferation potential was evaluated after 24 and 72 h of the cell culture according to the manufacturer's protocol. The absorbance at 450 nm was measured with a microplate reader Multiskan FC (Thermo Fisher Scientific, Waltham, MA, USA). hUC-MSCs cultured on TC-treated polystyrene surface (TCPS) in standard medium were used as a control.

Results and discussion

Thermal characterization: differential scanning calorimetry (DSC) and thermogravimetric analysis (TGA)

DSC curves (Fig. 1) of the prepared hydrogels exhibit two main endothermic peaks. The first one at temperature ca. 0 °C is associated to the melting of non-bonded or weakly bonded water, which freezes during the cooling at the beginning of the measurement. This peak is divided into two smaller ones. The sharp one corresponds to free water; while, the broad one to freezing bound water.

Generally, in hydrogels, there are three types of water: free water, freezing bound water and non-freezing bound water. Free water does not form hydrogen bonds with the macromolecules and behaves similarly as pure water with freezing and melting transitions. Freezing bound water interacts weakly with macrochains and freezes/melts at temperatures shifted compared to that of free water. Non-freezing bound water is linked to the macrochains only by hydrogen bonds, and does not undergo phase transitions within the normal temperature range typical to water [27–29]. The information on different types of water in polymer hydrogels is crucial for assessment and understanding the adsorption/desorption processes in hydrogels and their biocompatibility [30]. In order to evaluate the content of non-bonded or weakly bonded water (W_f) within the hydrogels, Eq. 6 was used:

$$W_f = \left(\frac{\Delta H_{melting}}{\Delta H_{water}} \right) \cdot 100 [\%] \tag{6}$$

where: W_f—content of non-bonded or weakly bonded water, $\Delta H_{melting}$ is the area under the first melting peak and ΔH_{water} is the heat of fusion of pure water and is equal to 333.3 [J g^{-1}]. All the results are presented in Table 2.

Based on the results from Table 2, it can be concluded that composites with hydroxyapatite exhibit lower water content with respect to the ones with GO. It is evidenced by the values of the heat of fusion for both endothermic peaks. The lowest values were obtained for the SA+2%HAp and SA+5%HAp samples. For samples with HAp, the ratio between freezing water and free water content (calculated
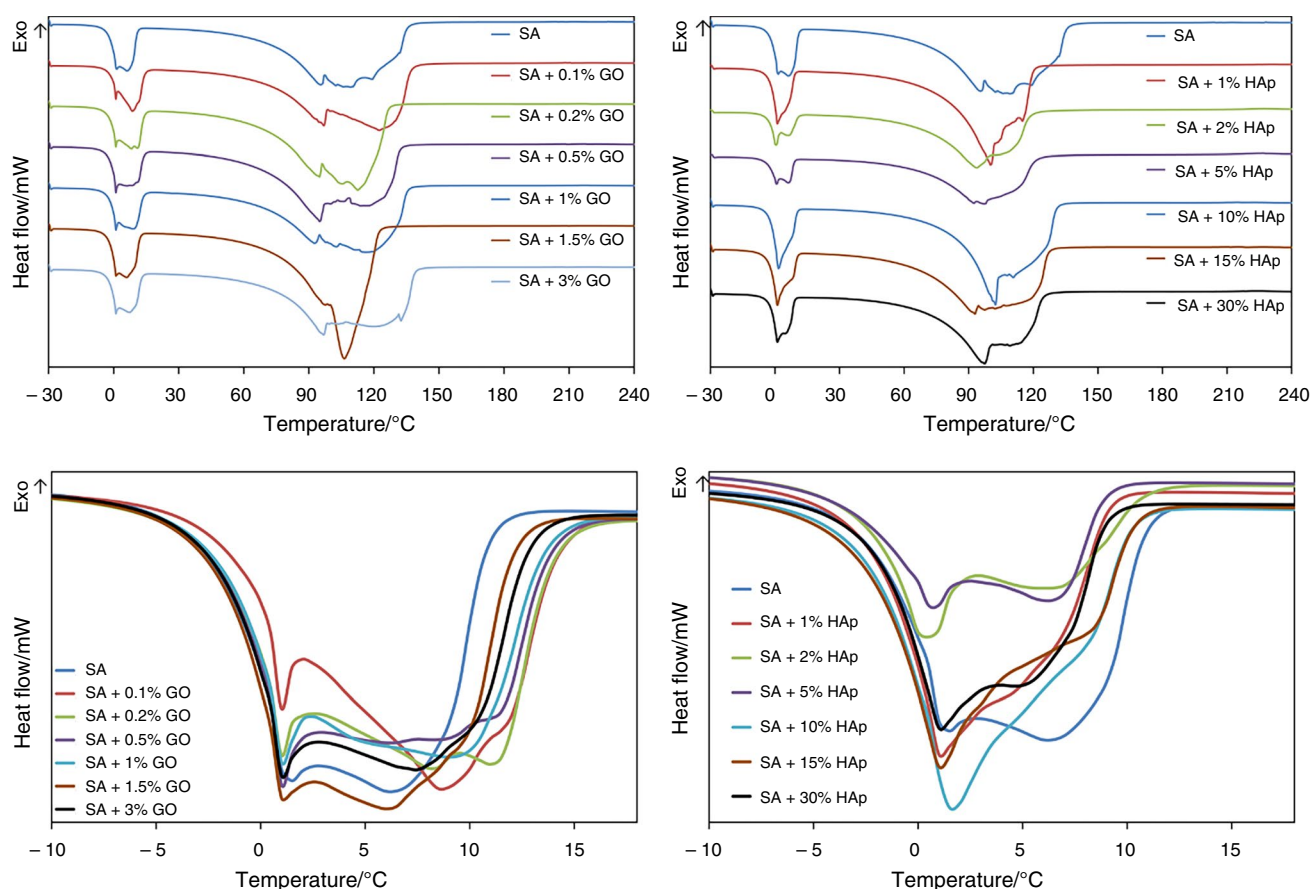
Fig. 1 DSC curves for manufactured samples with the detailed curves for melting of non-structured water (below): **a** SA/GO hydrogels; **b** SA/ HAp hydrogels

Table 2 DSC parameters for the obtained hydrogels

Sample	First peak					Second peak		
	T_{max1}/°C	T_{max2}/°C	Heat/J g^{-1}	W_f %	$W_{freezing}$/W_{free}	T_{max1}/°C	T_{max2}/°C	Heat/J g^{-1}
SA	1	6	294	88.3	0.90	94	108	2015
SA+0.1%GO	1	8	288	86.5	2.53	96	121	2020
SA+0.2%GO	0	8	316	94.9	1.82	93	111	2148
SA+0.5%GO	0	6	304	91.3	1.58	93	117	2097
SA+1%GO	1	8	302	90.7	1.79	91	115	2072
SA+1.5%GO	1	5	333	100.0	1.24	96	104	2306
SA+3%GO	0	7	303	91.0	1.40	96	118	2069
SA+1%HAp	0	-	264	79.3	0.43	98	132	1873
SA+2%HAp	0	5	176	52.8	0.72	93	102	1367
SA+5%HAp	0	6	148	44.4	0.49	92	96	1203
SA+10%HAp	1	-	275	82.6	0.37	101	98	1886
SA+15%HAp	1	-	279	83.8	0.45	92	93	1923
SA+30%HAp	1	-	228	68.5	0.54	96	95	1597

using OriginPro software as a ratio of the area under the peaks) is much lower than in the case of SA/GO hydrogels. These findings stay in good agreement with calculated energy of hydrogen bonds presented in Table 4. The

obtained results suggest stronger interactions between polymer chains and HAp that lead to bonding of lower amounts of water in comparison with hydrogels modified with GO. Moreover, composites modified with HAp exhibit few

times lower content of freezing bound water with respect to free water, which may suggest that GO facilitates confinement of water molecules between GO nanoparticles and SA macrochains due to stronger hydrogen interactions. For SA/HAp hydrogels, higher content of water, especially free water, was found. For the second endothermic peaks at ca. 90–120 °C, the temperature shifts after incorporation of the nanoadditive. It can be seen that for hydrogels modified with GO endothermic peaks at ca. 90–120 °C were shifted to the higher temperature, while for hydrogels modified with HAp to lower temperatures in comparison with unmodified SA. This effect can be attributed to the ratio of freezing and free water. In hydrogels modified with GO more water was hydrogen-bonded as freezing water, while for hydrogels modified with HAp more water was found as free water. Free water can easily evaporate from hydrogel at lower temperature; while, hydrogen-bonded water evaporates at higher temperature.

TG results (Fig. 2, Table 3) show that hydrogels undergo a water evaporation in the temperature range 30–150 °C. At higher temperatures of 190–270°C, the second and much smaller mass loss can be observed connected to the thermal decomposition of sodium alginate. Based on the curves, it is noticeable that an addition of GO (Fig. 2a) as well as HAp (Fig. 2b) expands temperature range of water evaporation. The changes are bigger in the case of SA/GO hydrogels, even up to 40 °C.

TG parameters (Table 3) confirm that nanoadditives shift water evaporation temperature toward higher values. In the case of GO, the values are varying—no clear dependency occurs. On the one hand, GO causes moving apart of polymeric chains (which simplifies water evaporation), but, on the other hand, GO flakes may be a physical barrier for water molecules inside the material. In general, SA/GO hydrogels contained more water than SA/HAp ones. During the second

step, a decrease in sample mass starts faster in the case of composite hydrogels. It shows that nanoadditives incorporation leads to decrease in thermal stability of an alginate matrix due to the moving apart of polymer chains.

Spectroscopic analysis (FTIR)

The results of FTIR analysis are shown in Fig. 3. Typical functional groups of sodium alginate were found. The biggest absorption band at 3423 cm^{-1} is related to the stretching of structural –OH groups in alginate. Other important bands observed at 1617 cm^{-1} and 1427 cm^{-1} are related to, respectively, asymmetric and symmetric stretching of C=O in carbonyl groups. The triplet of bands at 1122 cm^{-1}, 1087 cm^{-1} and 1032 cm^{-1} (Fig. 3c and e) is characteristic for ether group in the saccharide structure of alginate [31].

The band at ca. 1122 cm^{-1} is associated with the stretching of C–O from the crystalline region of the alginate chains. Based on the position of the band from bonded –OH groups at ca. 3420 $cm.^{-1}$ (Fig. 3d and Fig. 3f), the distance between –OH and O can be evaluated. This distance (R) was calculated using the Pimentel–Sederholm equation [32] (Eq. 7)

$$\Delta\upsilon = 4430 \cdot (2.84 - R)[cm^{-1}] \tag{7}$$

where $\Delta\upsilon = \upsilon_{bondedOH} - \upsilon_{freeOH}$ and $\upsilon_{freeOH} = 3650$ [cm^{-1}].

The energy of the hydrogen bond (E_H) was calculated using the Eq. (8):

$$E_H = 1/K \cdot (\upsilon_{freeOH} - \upsilon_{bondedOH})/\upsilon_{freeOH}[kcal] \tag{8}$$

Where K is a constant equal to 1.6 10^{-2} kcal [33, 34]. Calculated parameters are presented in Table 4.

The addition of GO (Fig. 3a) and HAp (Fig. 3b) into polymeric matrix causes a big intensity decrease in the bands, which is stronger in the case of SA/GO hydrogels, because
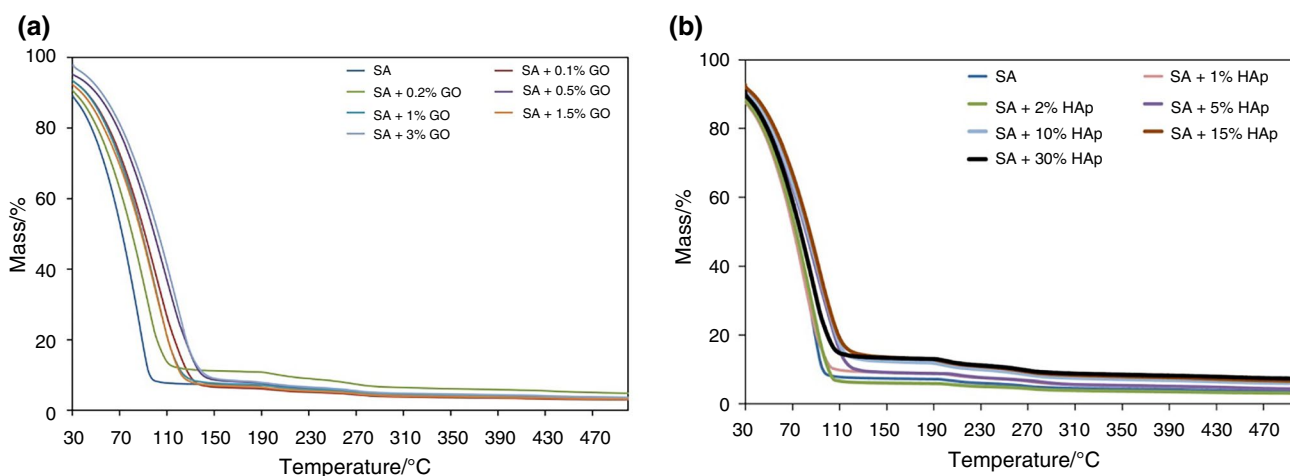

Fig. 2 TG curves for manufactured samples: **a** SA/GO hydrogels; **b** SA/HAp hydrogels

Table 3 TGA parameters of obtained hydrogels

Sample	Water evaporation					Chains decay				
	$T_{5\%}$/°C	$T_{10\%}$/°C	T_{endset}/°C	DTG_{max}/°C	Mass loss/%	$T_{3\%}$/°C	$T_{5\%}$/°C	$T_{10\%}$/°C	DTG_{max1}/°C	DTG_{max2}/°C
SA	37	45	95.6	88	91.9	198	201	210	203	265
SA+0,1%GO	43	53	125.6	102	92.9	189	193	204	205	269
SA+0,2%GO	39	48	106.2	95	87.8	194	197	207	198	268
SA+0,5%GO	48	58	133.1	108	91.6	186	191	201	200	270
SA+1%GO	43	52	118.8	100	91.6	189	193	202	199	272
SA+1,5%GO	42	51	119.6	99	92.6	188	192	202	194	271
SA+3%GO	47	58	134.5	119	91.2	184	189	199	181	271
SA+1%HAp	38	45	95.6	80	89.8	197	210	210	203	272
SA+2%HAp	37	45	100.3	86	93.1	199	203	213	206	272
SA+5%HAp	39	48	119.1	89	89.9	204	208	218	209	284
SA+10%HAp	40	48	111.8	94	86.5	192	195	204	198	267
SA+15%HAp	41	50	110.5	94	85.1	190	194	203	193	265
SA+30%HAp	38	46	101.5	82	85.3	196	200	210	200	265

GO acts like black-body material and absorbs a large part of the radiation. The interaction between alginate and nanoadditives is visible through the shift of the bands at 3423 cm^{-1} and 1617 cm^{-1} to the higher wavenumbers. It indicates that GO, as well as HAp, made alginate chains move apart from each other, which weakened hydrogen bonding in the polymer matrix. Stronger hydrogen bonds in hydrogels modified with HAp can be observed, which can be connected to the polar nature of HAp and leads to stronger interactions between polymer chains and HAp nanoparticles. For samples with 10%, 15% and 30% of HAp, a small band at ca. 600 cm^{-1} corresponding to O–P–O stretching can be observed.

Mechanical properties

Based on the results of the mechanical tests (Fig. 4) it can be seen that incorporation of nanoadditives changes mechanical properties of the hydrogels.

In the case of SA/GO (Fig. 4a, b), Young's moduli of the composites with 0.1% and 0.2% of GO were similar or slightly lower than for the unmodified SA (1.0 MPa). Better reinforcement effect was observed in a case of SA/HAp composites (Fig. 4c). Moreover, it was observed that the best mechanical properties were found for hydrogels after two weeks incubation in calcium chloride solution, because of the higher crosslinking density. However, after a longer time, incubation in calcium chloride solution can cause resubstitution of Na$^+$ and Ca^{2+} ions and formation of soluble sodium alginate which leads to the decrease in mechanical parameters. The most similar mechanical parameters to the native cartilage tissue were obtained for SA+0,5%GO after one week of incubation with compressive modulus ca. 1.1 MPa and Poisson's ratio around 0.54, and SA+15%HAp after two weeks of incubation with compressive modulus ca. 1.6 MPa and Poisson's ratio around 0.64. Based on the literature, the compressive modulus of cartilage tissue changes from 0.08 MPa for articular cartilage to 2.1 MPa for subchondral bone [35]; while, Poisson's Ratio of cartilage is 0.5 [5]. These results suggest to use SA/GO hydrogel near cartilage zone and SA/HAp hydrogel near subchondral bone zone, because of the changes of the mechanical properties throughout the tissue. Additionally, HAp incorporation can improve bioactivity of the hydrogel and regeneration of bone tissue [36].

Tribological properties

Based on Stribeck's curves (Fig. 5), it can be found that, by changing the amount of nanoadditives, the friction coefficient of the hydrogels can be changed.

For articular cartilage the friction coefficient is ca. 0.001 [5, 35], so in the case of biomaterials used for knee-joint,

Fig. 3 FTIR spectra for obtained SA/GO and SA/HAp hydrogels, respectively: **a**, **b** normalized spectra, **c**, **e** detailed spectra for the fingerprint region, and **d**, **f** detailed spectra for –OH and –CH groups
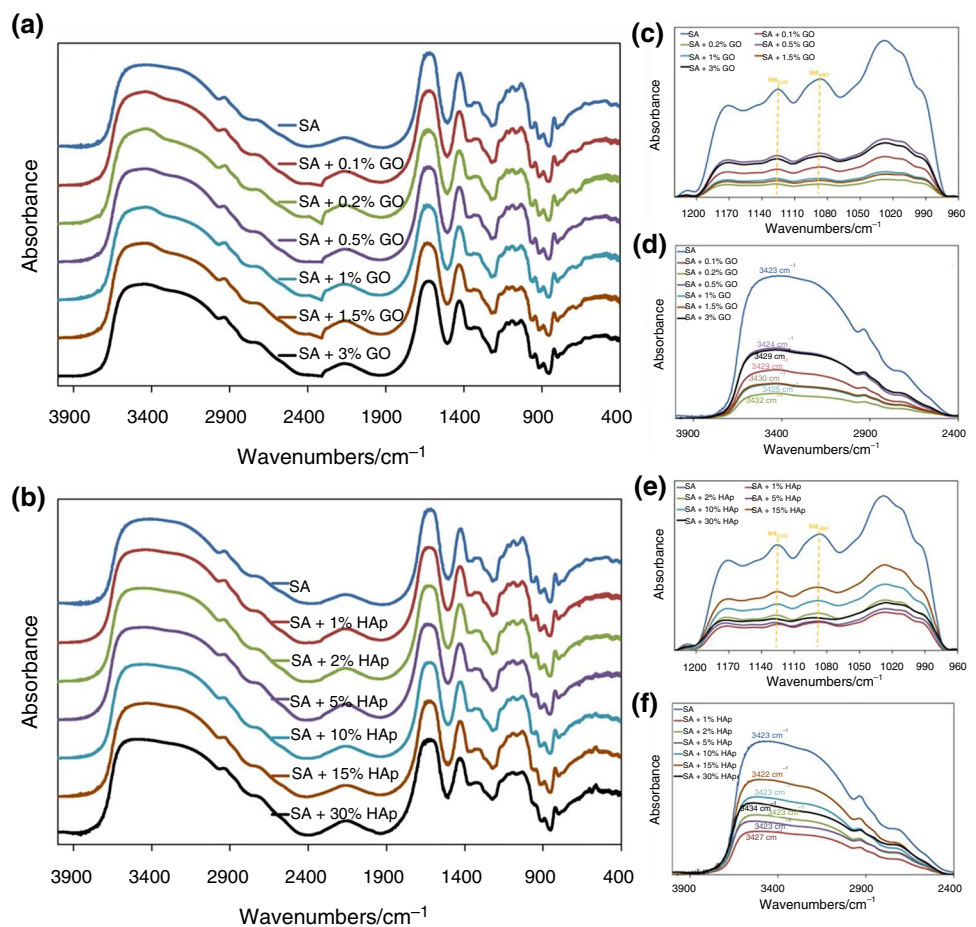
Table 4 Distance between –OH and O (R) and the energy of the hydrogen bond (E_H)

Sample	R/Å	E_H/kcal
SA	2.891	3.884
SA + 0.1%GO	2.890	3.781
SA + 0.2%GO	2.889	3.727
SA + 0.5%GO	2.891	3.864
SA + 1%GO	2.891	3.855
SA + 1.5%GO	2.890	3.775
SA + 3%GO	2.890	3.789
SA + 1%HAp	2.890	3.824
SA + 2%HAp	2.891	3.886
SA + 5%HAp	2.891	3.887
SA + 10%HAp	2.891	3.895
SA + 15%HAp	2.892	3.912
SA + 30%HAp	2.889	3.704

as small friction coefficient as possible is required. In the first region of sliding velocity up to 200 mm s^{-1}, some reinforced hydrogels show higher friction coefficient than unmodified SA. Probably, at the beginning of the analysis

(during the run-in period of the test), nanoadditives were not well-arranged yet and have direct contact with the measuring ball. After the initial part of the experiment, the friction coefficient decreased (to around 800 mm s^{-1} sliding velocity). In general, obtained hydrogels showed very low friction coefficient, which was no higher than 0.04 throughout the analysis (except SA + 0, 1%GO sample at the highest sliding velocity), however was higher than for articular cartilage. Similar effect with higher friction coefficient at the beginning of measurement has been observed by Wang et al. [37] in polyacrylamide (PAAm) hydrogels modified with GO. Authors suggested that introducing GO flakes to PAAm hydrogels reinforces the bearing capacities of these materials. Moreover, no correlation between the friction coefficient and GO content was found. In the investigated SA/GO systems similar effect can be taken into account—functional groups from GO can interact with polar groups in SA macrochains and reinforce hydrogel by forming a network. In consequence, at the beginning of measurement the friction coefficient can be higher as in hydrogel stronger interaction occurs. After breaking these interactions, as well as due to graphene nanosheets sliding, the friction coefficient decreases. Friction coefficient of SA/GO systems depends
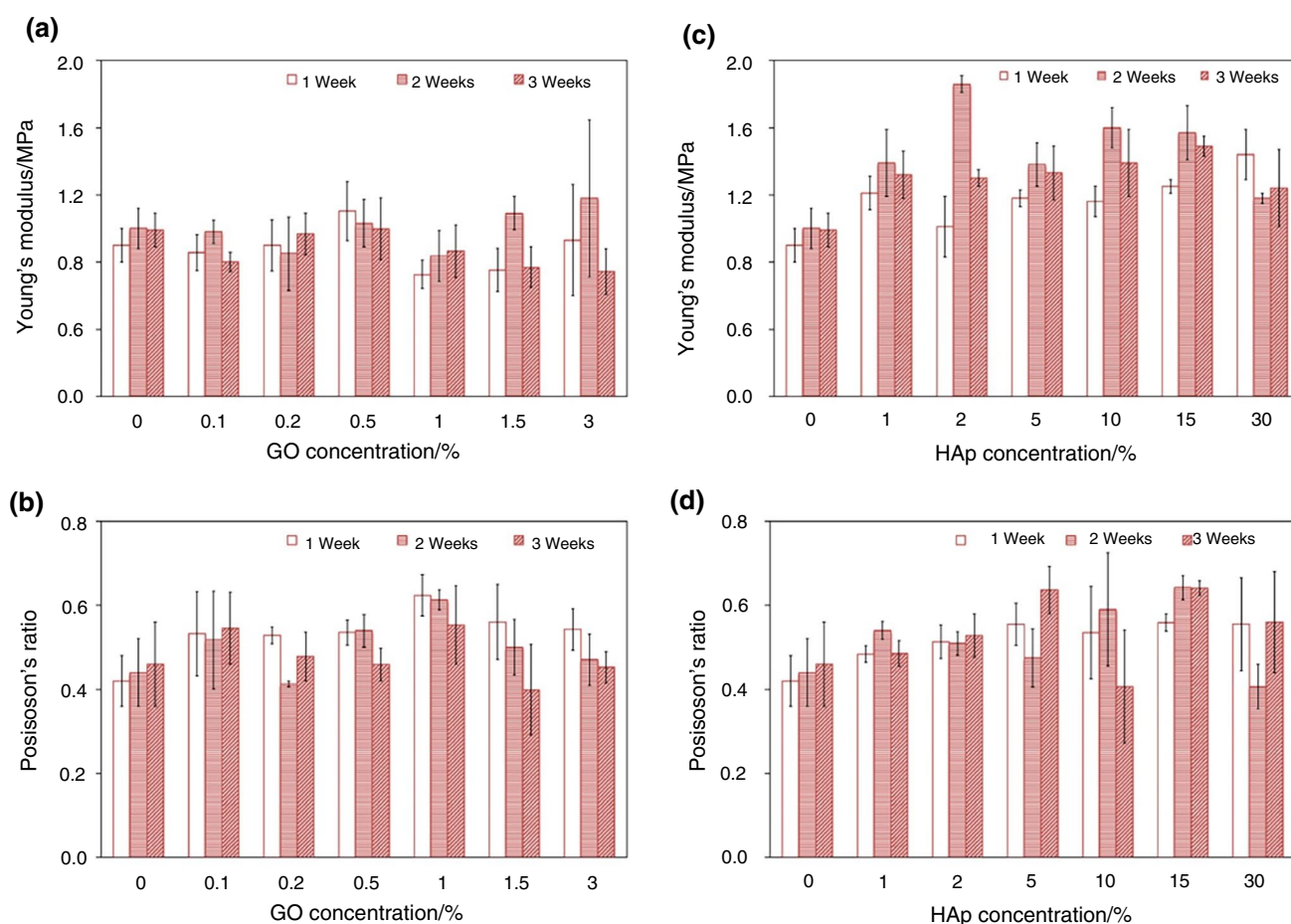
Fig. 4 Young's modulus (upper row) and Poisson's ratio (lower row) of the hydrogels in the function of the nanoadditives content and crosslinking time: **a**, **b** SA/GO hydrogels; **c**, **d** SA/HAp hydrogels. The bars represent mean ± SD (*n* ≥ 3)
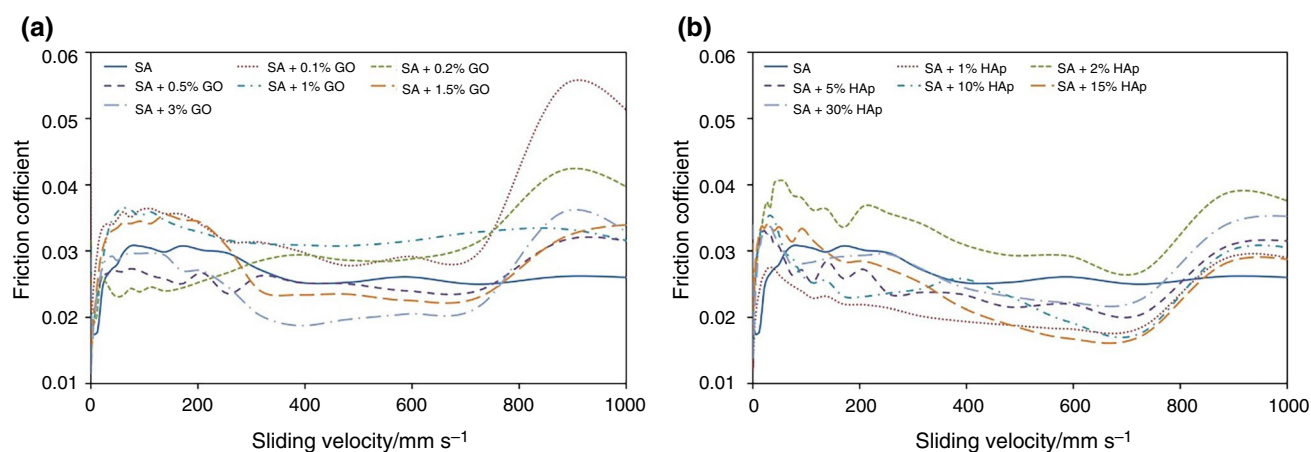

Fig. 5 Friction coefficient of manufactured hydrogels in the function of the sliding velocity: **a** SA/GO hydrogels; **b** SA/HAp hydrogels

on both SA and GO interactions, but also on GO dispersion in SA matrix, viscosity of SA/GO systems and tendency to GO agglomeration, especially for higher GO content. That

can explain lack of correlations between friction coefficient and GO content.

The lowest friction coefficient was observed for hydrogel modified with 3% of GO. Similar effect was observed by Shi

et al. [38] where in poly(vinyl alcohol) hydrogels decreasing in friction coefficient with increasing of GO content has been found. They postulated that hydrogel can be considered as a biphasic material due to its porous structure with large water amount. It was postulated that the incorporation of GO leads to the improvement in the hydrophily of the hydrogel composites. Water-locking and fluid load supports during sliding and results in the low friction. Moreover graphene and graphene oxide are well-known 2D nanolubricants and ultra-high-speed superlubricity of micrometer-sized graphene flakes has been observed [39, 40]. Feng et al. [41] found that sliding of graphene nanosheets depends on the temperature. Mechanism of graphene nanosheets sliding includes translational and rotational motions in the initial and final states in addition to which a commensurate–incommensurate transition occurs in the graphene sliding mechanism [42].

Microscopic observations (SEM)

In order to observe a microstructure, SEM microphotographs of the lyophilized sample's fracture were performed for obtained hydrogels (Fig. 6).

Obtained hydrogels show porous structure. The pore distribution is not homogenous and changes with an amount of incorporated nanoadditives. The pore sizes vary from around 150 to 400 µm. In case of SA/HAp hydrogels (Fig. 6c), the presence of bioceramic is visible on the materials surface.

Chemical stability under in vitro conditions

Next, investigations of moisture uptake and in vitro chemical stability were performed. It was assumed, that obtained material will be implanted to the body not in the dry form but in the form of hydrogel, and the swelling degree was determined for the hydrogel. This was performed to find the swelling ability in the presence of other fluids, such as PBS and Ringer solution, and to check the potential hydrogel behavior in contact with physiological fluids. The swelling degree (SD) was investigated for all the samples incubated in PBS and Ringer solution. SD was calculated according to Eq. 9:

$$SD = \frac{m_{wet} - m_{initial}}{m_{initial}} \cdot 100 [\%] \tag{9}$$

Fig. 6 SEM microphotographs of SA (**a**), SA/GO (**b**), and SA/HAp (**c**) hydrogels

Where $m_{initial}$ is the mass of the hydrogel before the incubation and m_{wet} is the mass of the hydrogel after a certain period of incubation. Before the weighting, the samples were superficially dried in order to remove excess liquid from the surface. The results are presented in Fig. 7. The fifth order polynomial regression line was generated using Microsoft Excel software.

Based on the results, equilibrium swelling degree (ESD) was also calculated as:

$$ESD = \frac{m_{wetend} - m_{initial}}{m_{initial}} \qquad (10)$$

Where m_{wetend} was calculated as an average value from the three last testing points.

The results are given in Fig. 11.

Based on the ESD values (Fig. 8), it can be concluded that hydrogels exhibit higher swelling degree in PBS solution. Also, all GO-modified hydrogels were more susceptible to swelling in Ringer solution as compared to unmodified hydrogel (SA). The samples with 0.5% and 1% of GO had higher ESDs in PBS than the control (Fig. 8a). The

addition of HAp did not change the hydrogels behavior during the incubation – ESDs of the samples were similar as ones of pure SA (Fig. 8b). Also, for SA/HAp hydrogels, the ESD in Ringer solution was few times lower than for SA/GO.

Also, in the case of pH, the biggest changes occurred during the first four days of the experiment. In case of incubation in PBS, pH decreased from 7.2 to 5.4 in case of both graphene- (Fig. 9a) and hydroxyapatite modified (Fig. 9c) hydrogels.

Next, pH was almost constant. In some cases, by the end of the analysis, white precipitate occurred, which was connected with the slight increase in pH. It can be connected with the degradation process of hydrogels and $CaCl_2$ precipitation.

Also pH of Ringer solution (Fig. 9b, d) decreased after the first four days of incubation. Although, this change was considerably smaller than in the case of PBS solution (from 7.0 to around 6.0), SA/GO samples (Fig. 9b) did not show any significant changes with respect to SA hydrogel. Based on FTIR results it can be observed that interaction between SA and HAp are stronger than interactions between SA and
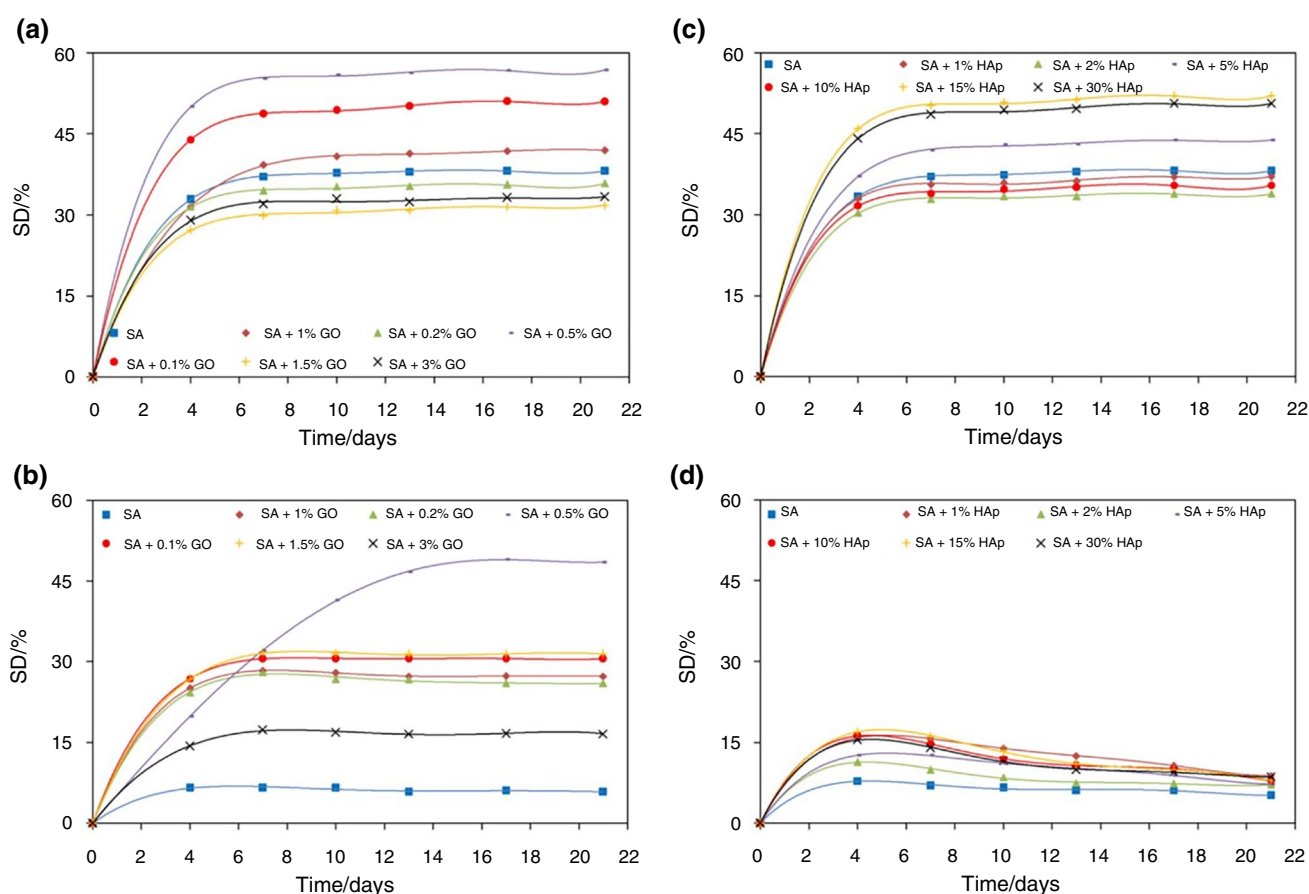

Fig. 7 Swelling kinetics in PBS (upper row) and Ringer's (lower row) solution for the obtained hydrogels: **a**, **b** SA/GO hydrogels; **c**, **d** SA/HAp hydrogels
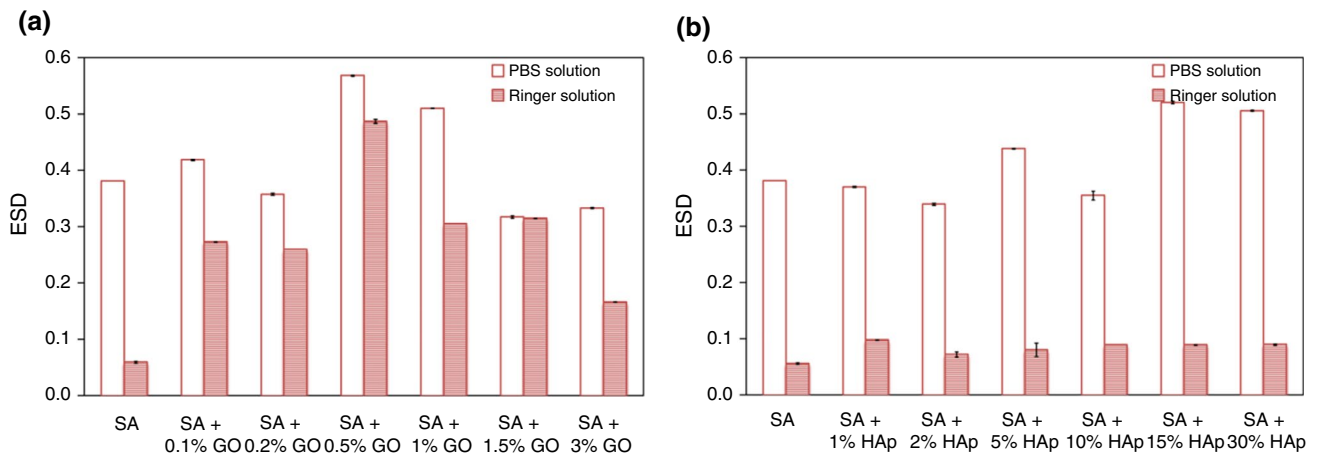
Fig. 8 Equilibrium swelling degree (ESD) for obtained hydrogels in different aqueous media: **a** SA/GO hydrogels; **b** SA/HAp hydrogels. The bars represent mean ± SD ($n=3$)
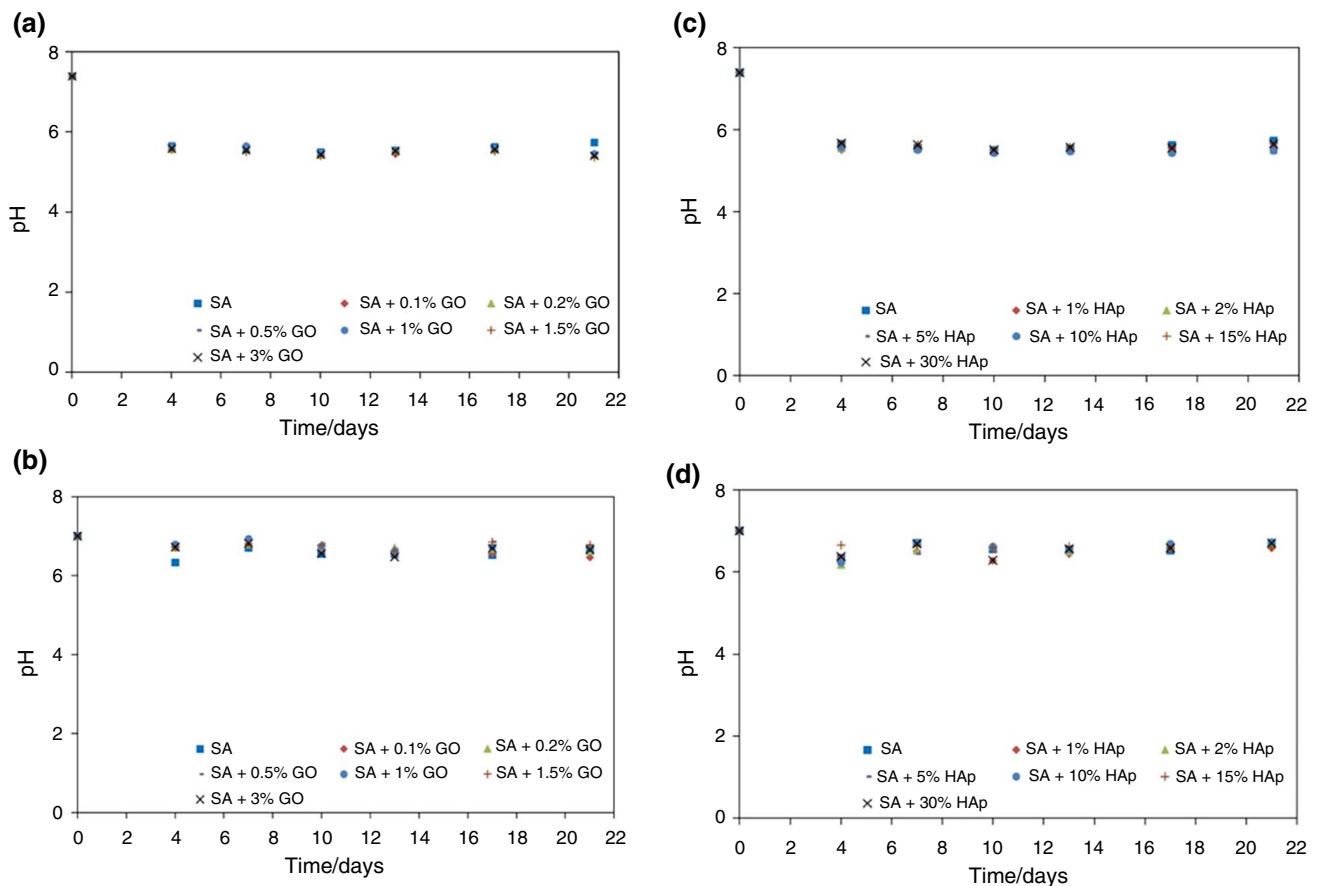

Fig. 9 pH changes during incubation in PBS (upper row) and Ringer's (lower) solution for obtained hydrogels: **a**, **b** SA/GO hydrogels; **c**, **d** SA/HAp hydrogels

GO. However, during incubation in water-based fluids HAp undergoes dissociation and gradually passes to the solution that leads to slight increase in pH, while in hydrogels such effect was not observed. That suggests higher chemical stability of SA/GO hydrogels.

Biological studies

The phenotypic analysis showed that isolated hUC-MSCs present high expression of MSCs specific surface markers including CD29, CD73, CD90 and CD105. Simultaneously, the cells did not express surface markers characteristic for hematopoietic stem cells (CD34) and immune cells (CD14, CD16, HLA-DR). Representative graphs from flow cytometry analysis are presented in Fig. 10.

In the biological part of the research, the impact of particles released from the alginates on the basic functional properties of hUC-MSCs was evaluated. The experimental group for biological analysis was reduced from six to three samples per experimental group. The samples chosen for the reduced experimental group were these with the lowest and the highest content of both GO and HAp additive. The third sample contained the middle value of an additive. By choosing those three additive loads, it was assumed to get the representative view at the property's changes vs materials composition. The cytotoxicity test (LDH Cytotoxicity Detection Kit; Roche Diagnostics, Rotkreuz, Switzerland) was performed after 24 h and results are presented in Fig. 11 as a percentage of the level of LDH released from the untreated control cells. Four independent repetitions of the test were performed. The results demonstrated that hUC-MSCs cultured in alginate extract of SA + 1%HAp released the highest level of LDH, which is statistically significant relative

to the control conditions (67% more than cells cultured in control medium, named as TCPS). Interestingly, in other tested conditions, no significant changes in the level of LDH were observed. However, higher level of LDH was noted in SA/HAp hydrogels compared to SA/GO hydrogels. It can be associated with lower water content in SA/HAp hydrogels compared to SA/GO hydrogels, which is confirmed by the results summarized in Table 2. The significant increase in the LDH may also suggest the beginning of the cell differentiation process, which is associated with the decrease in the cell proliferation. Therefore, further experiments are
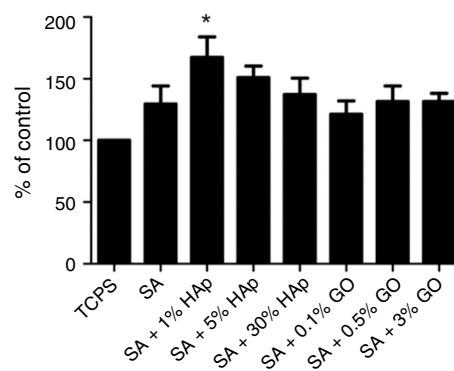

Fig. 11 Cytotoxicity of alginate-based extracts toward hUC-MSCs after 24 h of cell culture
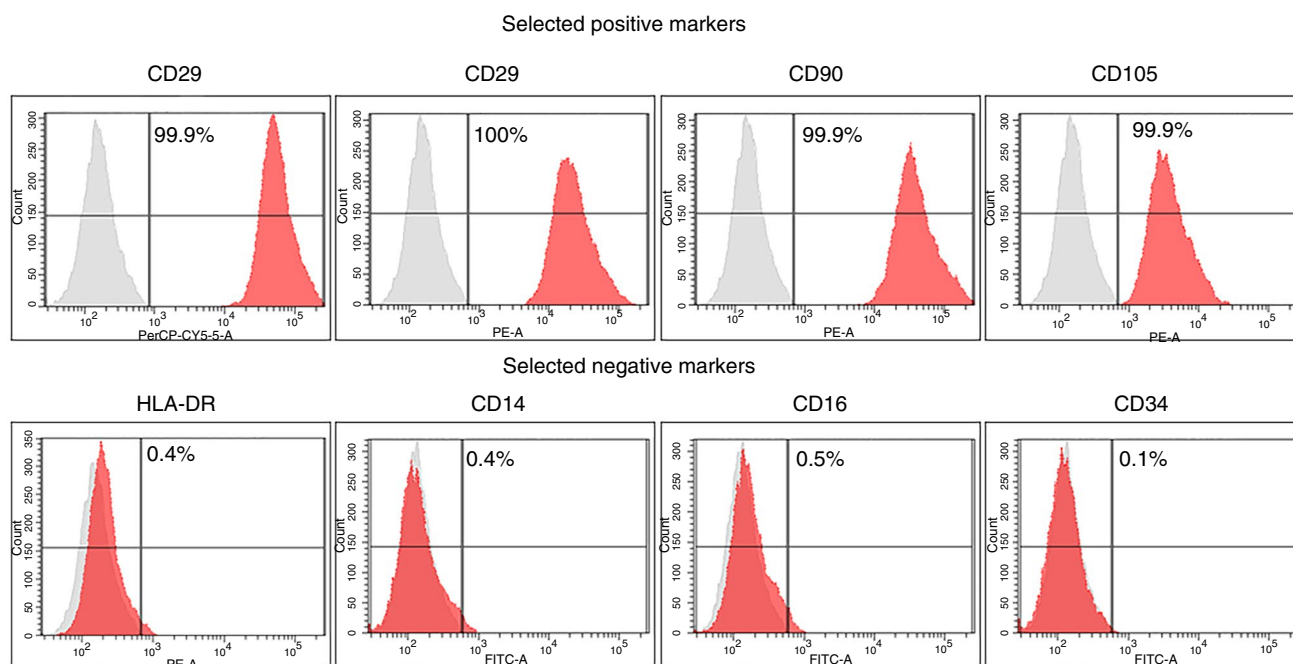

Fig. 10 Flow cytometry analysis of hUC-MSCs phenotype. Representative histograms showing the expression of selected positive and negative surface markers. Each histogram consist of overlayed signal for control unstained cells (gray) and signal for cells stained with fluores-cently conjugated antibodies against indicated surface markers (red). The numbers on the histograms represent the percentage of cells positive for particular antigen (percentage of cells with fluorescence signal above the autofluorescence of unstained control)

Fig. 12 Proliferation of hUC-MSCs after 24 h and 72 h of cell culture in alginate-based extracts
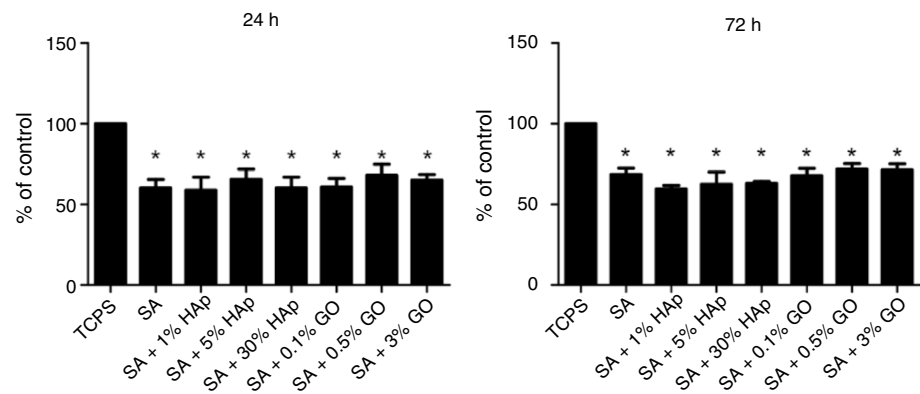
required to analyze the impact of the alginate extracts on hUC-MSCs differentiation to explain this phenomenon.

The proliferation assay (Cell Counting Kit-8; Sigma-Aldrich, St. Louis, MI, USA) was performed after 24 h and 72 h of cell culture in particular alginate-based extract. The results are presented in Fig. 12 and expressed as a percentage of the control conditions (untreated cells, named as TCPS). Four independent repetitions of the test were performed. We revealed a significant decrease in proliferation rate of hUC-MSCs cultured in all types of alginate extracts in comparison with control cells (TCPS). However, we observed no differences between extracts from SA modified with HAp and GO compared to the pure SA.

Conclusions

Alginate-based composite hydrogels crosslinked with calcium ions were obtained. Two types of the nanoadditives were used to modify the polymer matrix, namely graphene oxide and hydroxyapatite. These nanocomponents affected the thermal properties of the hydrogels, as evidenced by thorough DSC and TG analysis. For composites with HAp, the ratio between freezing water and free water content was found to be much higher than in the case of SA/GO hydrogels. Moreover, composites modified with nanoceramics exhibit few times higher content of freezing water with respect to free water. Moreover, mechanical analysis showed that the amount of the nanoadditives as well as incubation time influence properties of the hydrogels. Tribological analysis proved that friction coefficient of the tested hydrogels was very low. Based on the FTIR analysis, weakening of hydrogen bonding in the alginate structure was found. All the hydrogels were stable under in vitro conditions. The biological experiments demonstrated that most of the investigated hydrogels extracts are not cytotoxic toward hUC-MSCs.

Among the manufactured SA/GO hydrogels, the most promising properties for biomedical applications were observed in the SA + 0,5% GO sample. It exhibited mechanical properties similar to natural cartilage, a relatively low friction coefficient, and advantageous thermal properties (as compared to bare SA). In biological studies, the best results were achieved with a graphene oxide content of 0.5%. Among the manufactured HAp-modified hydrogels, the most promising mechanical properties were observed in the SA + 15% HAp sample. Structural studies by FTIR revealed that in this material the bond between HAp and SA was the strongest.

Author contributions Conceptualization contributed by Ewa Zuba-Surma, Kinga Pielichowska; investigation contributed by Aleksandra Lach, Monika Skoczeń, Klaudia Ordon, Patrycja Domalik-Pyzik, Sylwia Noga, Małgorzata Sekuła-Stryjewska, Elżbieta Karnas, Aleksandra Byrska, Joanna Jagiełło, Ludwika Lipińska; writing—original draft preparation contributed by Aleksandra Lach, Sylwia Noga, Kinga Pielichowska; writing—review and editing contributed by Patrycja Domalik-Pyzik, Ludwika Lipińska, Sylwia Noga, Ewa Zuba-Surma, Kinga Pielichowska; supervision contributed by Ewa Zuba-Surma, Kinga Pielichowska; funding acquisition contributed by Ludwika Lipińska, Patrycja Domalik-Pyzik, Ewa Zuba-Surma. All authors read and approved the final manuscript.

References

1. Korpayev S, Kaygusuz G, Şen M, Orhan K, Oto Ç, Karakeçili A. Chitosan/collagen based biomimetic osteochondral tissue constructs: a growth factor-free approach. Int J Biol Macromol. 2020;156:681–90. https://doi.org/10.1016/J.IJBIOMAC.2020.04.109.

2. Gadjanski I, Vunjak-Novakovic G. Challenges in engineering osteochondral tissue grafts with hierarchical structures. Expert Opin Biol Ther. 2015;15(11):1583–99. https://doi.org/10.1517/14712598.2015.1070825.

3. Rho J-Y, Kuhn-Spearing L, Zioupos P. Mechanical properties and the hierarchical structure of bone. Med Eng Phys. 1998;20(2):92–102. https://doi.org/10.1016/S1350-4533(98)00007-1.

4. Chung EJ, Shah N, Shah RN. Nanomaterials for cartilage tissue engineering. Nanomater Tissue Eng Fabr Appl. 2013. https://doi.org/10.1533/9780857097231.2.301.

5. Mansour JM. "Biomechanics of cartilage. Kinesiol Mech Pathomech. 2003;2:66–75.

6. Vedadghavami A, et al. Manufacturing of hydrogel biomaterials with controlled mechanical properties for tissue engineering applications. Acta Biomater. 2017;62:42–63. https://doi.org/10.1016/J.ACTBIO.2017.07.028.

7. Venkatesan J, Nithya R, Sudha PN, Kim SK. Role of alginate in bone tissue engineering. Adv Food Nutr Res. 2014;73:45–57. https://doi.org/10.1016/B978-0-12-800268-1.00004-4.

8. Venkatesan J, Bhatnagar I, Manivasagan P, Kang KH, Kim SK. Alginate composites for bone tissue engineering: a review. Int J Biol Macromol. 2015;72:269–81. https://doi.org/10.1016/J.IJBIOMAC.2014.07.008.

9. Al-Sabah A, et al. Structural and mechanical characterization of crosslinked and sterilised nanocellulose-based hydrogels for cartilage tissue engineering. Carbohydr Polym. 2019;212:242–51. https://doi.org/10.1016/J.CARBPOL.2019.02.057.

10. Stagnaro P, Schizzi I, Utzeri R, Marsano E, Castellano M. Alginate-polymethacrylate hybrid hydrogels for potential osteochondral tissue regeneration. Carbohydr Polym. 2018;185:56–62. https://doi.org/10.1016/J.CARBPOL.2018.01.012.

11. Radhakrishnan J, Manigandan A, Chinnaswamy P, Subramanian A, Sethuraman S. Gradient nano-engineered in situ forming composite hydrogel for osteochondral regeneration. Biomaterials. 2018;162:82–98. https://doi.org/10.1016/J.BIOMATERIALS.2018.01.056.

12. Ruvinov E, Tavor Re'em T, Witte F, Cohen S. Articular cartilage regeneration using acellular bioactive affinity-binding alginate hydrogel: a 6-month study in a mini-pig model of osteochondral defects. J Orthop Transl. 2019;16:40–52. https://doi.org/10.1016/J.JOT.2018.08.003.

13. Montalbano G, et al. Synthesis of bioinspired collagen/alginate/fibrin based hydrogels for soft tissue engineering. Mater Sci Eng C. 2018;91:236–46. https://doi.org/10.1016/J.MSEC.2018.04.101.

14. Zhu Y, et al. An injectable continuous stratified structurally and functionally biomimetic construct for enhancing osteochondral regeneration. Biomaterials. 2019;192:149–58. https://doi.org/10.1016/J.BIOMATERIALS.2018.11.017.

15. Nie L, Liu C, Wang J, Shuai Y, Cui X, Liu L. Effects of surface functionalized graphene oxide on the behavior of sodium alginate. Carbohydr Polym. 2015;117:616–23. https://doi.org/10.1016/J.CARBPOL.2014.08.104.

16. Marrella A, Lagazzo A, Barberis F, Catelani T, Quarto R, Scaglione S. Enhanced mechanical performances and bioactivity of cell laden-graphene oxide/alginate hydrogels open new scenario for articular tissue engineering applications. Carbon N Y. 2017;115:608–16. https://doi.org/10.1016/J.CARBON.2017.01.037.

17. Serrano-Aroca Á, Iskandar L, Deb S. Green synthetic routes to alginate-graphene oxide composite hydrogels with enhanced physical properties for bioengineering applications. Eur Polym J. 2018;103:198–206. https://doi.org/10.1016/J.EURPOLYMJ.2018.04.015.

18. Ionita M, Pandele MA, Iovu H. Sodium alginate/graphene oxide composite films with enhanced thermal and mechanical properties. Carbohydr Polym. 2013;94(1):339–44. https://doi.org/10.1016/J.CARBPOL.2013.01.065.

19. Shamekhi MA, Mirzadeh H, Mahdavi H, Rabiee A, Mohebbi-Kalhori D, Baghaban Eslaminejad M. Graphene oxide containing chitosan scaffolds for cartilage tissue engineering. Int J Biol Macromol. 2019;127:396–405. https://doi.org/10.1016/J.IJBIOMAC.2019.01.020.

20. Kucko NW, Herber RP, Leeuwenburgh SCG, Jansen JA. Calcium phosphate bioceramics and cements. Princ Regen Med. 2019. https://doi.org/10.1016/B978-0-12-809880-6.00034-5.

21. Jiang YY, et al. Preparation and enhanced mechanical properties of hybrid hydrogels comprising ultralong hydroxyapatite nanowires and sodium alginate. J Colloid Interface Sci. 2017;497:266–75. https://doi.org/10.1016/J.JCIS.2017.03.032.

22. Rajkumar M, Meenakshisundaram N, Rajendran V. Development of nanocomposites based on hydroxyapatite/sodium alginate: synthesis and characterisation. Mater Charact. 2011;62(5):469–79. https://doi.org/10.1016/J.MATCHAR.2011.02.008.

23. Huggins ML. The viscosity of dilute solutions of long-chain molecules. IV. Dependence on concentration. J Am Chem Soc. 1942;64(11):2716–8. https://doi.org/10.1021/ja01263a056.

24. Donnan FG, Rose RC. Osmotic pressure, molecular weight, and viscosity of sodium alginate. Can J Res. 1950;28(3):105–13. https://doi.org/10.1139/cjr50b-016.

25. Sakugawa K, Ikeda A, Takemura A, Ono H. Simplified method for estimation of composition of alginates by FTIR. J Appl Polym Sci. 2004;93(3):1372–7. https://doi.org/10.1002/APP.20589.

26. Jagiełło J, et al. Impact of graphene-based surfaces on the basic biological properties of human umbilical cord mesenchymal stem cells: implications for ex vivo cell expansion aimed at tissue repair. Int J Mol. 2019;20(18):4561. https://doi.org/10.3390/IJMS20184561.

27. Cursaru B, Stănescu PO, Teodorescu M. "The states of water in hydrogels synthesized from diepoxy-terminated poly(ethylene glycol)s and aliphatic polyamines." UPB Sci Bull Ser B Chem Mater Sci. 2010;72(4):99–114.

28. Hodge RM, Edward GH, Simon GP. Water absorption and states of water in semicrystalline poly(vinyl alcohol) films. Polymer. 1996;37(8):1371–6. https://doi.org/10.1016/0032-3861(96)81134-7.

29. Ahmad MB, Huglin MB. States of water in poly(methyl methacrylate-co-N-vinyl-2-pyrrolidone) hydrogels during swelling. Polymer. 1994;35(9):1997–2000. https://doi.org/10.1016/0032-3861(94)90995-4.

30. Gun'ko VM, Savina IN, Mikhalovsky SV. Properties of water bound in hydrogels. Gel. 2017;3(4):37. https://doi.org/10.3390/GELS3040037.

31. Van Hoogmoed CG, Busscher HJ, De Vos P. Fourier transform infrared spectroscopy studies of alginate–PLL

capsules with varying compositions. J Biomed Mater Res Part A. 2003;67A(1):172–8. https://doi.org/10.1002/JBM.A.10086.

32. Pimentel GC, Sederholm CH. Correlation of infrared stretching frequencies and hydrogen bond distances in crystals. J Chem Phys. 1956;24(4):639–41. https://doi.org/10.1063/1.1742588.

33. Zaltariov MF, Filip D, Varganici CD, Macocinschi D. ATR-FTIR and thermal behavior studies of new hydrogel formulations based on hydroxypropyl methylcellulose/poly(acrilic acid) polymeric blends. Cellul Chem Technol. 2018;52(7–8):619–31.

34. Croitoru C, Pop MA, Bedo T, Cosnita M, Roata IC, Hulka I. Physically crosslinked poly (Vinyl Alcohol)/kappa-carrageenan hydrogels: structure and applications. Polymers. 2020;12(3):560. https://doi.org/10.3390/POLYM12030560.

35. Dehghani F, Fathi A. Challenges for cartilage regeneration. Springer Ser Biomater Sci Eng. 2016;8:389–466. https://doi.org/10.1007/978-3-662-53574-5_14/COVER.

36. Pielichowska K, Blazewicz S. Bioactive polymer/hydroxyapatite (nano)composites for bone tissue regeneration. Adv Polym Sci. 2010;232(1):97–207. https://doi.org/10.1007/12_2010_50/COVER.

37. Wang C, Bai X, Guo Z, Dong C, Yuan C. A strategy that combines a hydrogel and graphene oxide to improve the water-lubricated performance of ultrahigh molecular weight polyethylene. Compos Part A Appl Sci Manuf. 2021;141: 106207. https://doi.org/10.1016/J.COMPOSITESA.2020.106207.

38. Shi Y, Xiong D, Li J, Wang N. The water-locking and cross-linking effects of graphene oxide on the load-bearing capacity of poly(vinyl alcohol) hydrogel. RSC Adv. 2016;6(86):82467–77. https://doi.org/10.1039/C6RA21272G.

39. Yang J, et al. Observation of high-speed microscale superlubricity in graphite. Phys Rev Lett. 2013;110(25): 255504. https://doi.org/10.1103/PHYSREVLETT.110.255504/FIGURES/3/MEDIUM.

40. Berman D, Erdemir A, Sumant AV. Graphene: a new emerging lubricant. Mater Today. 2014;17(1):31–42. https://doi.org/10.1016/J.MATTOD.2013.12.003.

41. Feng X, Kwon S, Park JY, Salmeron M. Superlubric sliding of graphene nanoflakes on graphene. ACS Nano. 2013;7(2):1718–24. https://doi.org/10.1021/NN305722D/SUPPL_FILE/NN305722D_SI_001.PDF.

42. Liu L, et al. Recent advances in friction and lubrication of graphene and other 2D materials: mechanisms and applications. Friction. 2019;7(3):199–216. https://doi.org/10.1007/s40544-019-0268-4.